ACS APPLIED MATERIALS & INTERFACES

RESEARCH ARTICLE

www.acsami.org

Formation of Through-Holes in Si Wafers by Using Anodically Polarized Needle Electrodes in HF Solution

Tomohiko Sugita, Chia-Lung Lee, Shigeru Ikeda, and Michio Matsumura*

Research Center for Solar Energy Chemistry, Osaka University, 1-3 Machikaneyama, Toyonaka, Osaka 560-8531, Japan

Supporting Information

ABSTRACT: Electrochemical pore formation in Si using an anodized needle electrode was studied. In the electrochemical process, a Pt, Ir or Pd needle with a diameter of 50−200 μm was brought into contact at its tip with a Si wafer, which was not connected to an external circuit, in HF solution. By applying an anodic potential to the needle electrode against a Pt counter electrode, a pore with a diameter slightly larger than the diameter of the needle electrode was formed in both p-type and n-type Si, of which current efficiency was higher for n-type Si. Through-holes were electrochemically formed in p-type and n-type Si wafers at speeds higher than 30 μm min^{-1} using a sharpened Ir needle electrode. A model was proposed to explain the results, in which the pore formation was attributed to successive dissolution of Si atoms near the 3-phase (Si/metal/HF solution) boundary by positive holes injected from the needle electrode to the surface of Si.

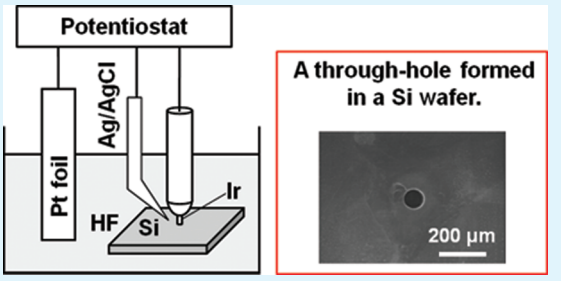

KEYWORDS: silicon, pore formation, through-hole, electrochemical etching, metal-assisted etching, catalyst

1. INTRODUCTION

Making minute through-holes in Si wafers is becoming an imortant processing technology for three-dimensional large-scale integration.[1,2] A typical technique for making through-holes in Si wafers is reactive ion etching,[3−6] in which reactive ions and radicals generated in a high-frequency electromagnetic field etch Si wafers at places uncovered with resist masks. Laser drilling is also an advanced technology for making through-holes, which does not need patterned masks. By this method, through-holes are made by pyrolytic excavation of Si at a place on which a condensed laser beam is focused.[7,8] Electrochemical machining of Si has also been studied.[9,10] In this process, a Si wafer is biased anodically and a fine needle electrode biased cathodically is brought close to the Si wafer in HF solution. Because of the electric resistivity of the HF solution, the anodic dissolution of Si proceeds selectively near the needle electrode and a pore is formed.

Another interesting method for making pores or etched patterns in Si is metal-assisted etching, which is reviewed in a recent paper.[11] In this process, a Si wafer on which particles of a metal such as Ag, Au or Pt are loaded is immersed in solution containing HF and an oxidant such as hydrogen peroxide. Because of the catalytic activity of the metals for transferring electrons from Si to the oxidant in solution, Si is easily etched. As a result, a so-called porous Si (PS) layer is formed on the surface. We found that under some conditions etching of Si proceeds at the Si/metal interface, which enables the formation of straight and helical pores in Si.[12−15] The pore size can be controlled from several tens of nm to a few μm depending on the size of metal particles used as the catalysts. If metal particles are densely loaded on Si wafers, the etching results in formation of nanowires of Si,[16−20] which grow through nanometer-sized gaps between the metal particles.

The metal-assisted etching is caused by metal particles to which a positive electrochemical potential is applied (or positive charge is donated) by oxidants included in HF solution.[11] Hence, it is theoretically possible to replace the metal particles and oxidants with electrodes biased anodically. In fact, we demonstrated electrochemical grooving and slicing of Si blocks using anodically biased Pt wires in HF solution.[21−23] This process is different from the conventional electrochemical machining of Si[9,10] using a cathodically biased needle electrode; we used Pt wires biased anodically against a counter electrode.

We have studied the formation of well-defined pores in Si wafers using fine needle electrodes biased anodically in HF solution. Using fine needle electrodes is convenient to make pores at desired places of Si wafers. It is also useful for obtaining reproducible current during the electrochemical process because of the easiness in making a Si/metal contact, which enables accurate analyses of the etching process with anodically biased electrode. Here, we report formation of through-holes in Si by this method. We also report the parameters affecting the electrochemical pore formation in Si, which include the electrochemical potentials applied to the needle electrodes and properties (conductive type and resistivity) of Si wafers. We consider that the results provide important insights into the mechanism of electrochemical etching and also metal-assisted etching of Si.

2. EXPERIMENTAL SECTION

Several kinds of Si wafers with (100) crystallographic orientation and resistivities of 0.1 to 230 Ω cm were purchased from Shin-Etsu Handoutai.

Received: March 16, 2011
Accepted: June 2, 2011
Published: June 02, 2011

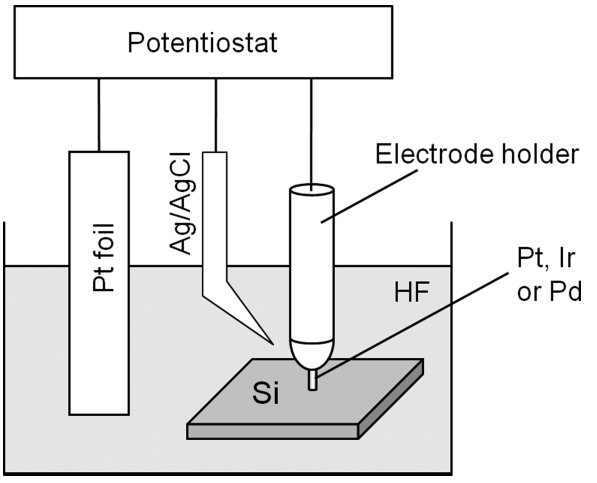

Figure 1. Setup of the electrochemical system for making a pore in Si.

The Si wafers were cut into 10 × 10 mm^2 square pieces and used as test samples and the electrochemical process was carried out on the mirror-polished surfaces. Prior to the experiment, the samples were cleaned by immersing in a mixture of hydrogen peroxide and sulfuric acid (30% H_2O_2: 97% H_2SO_4 = 1:4 in volume) for 10 min, rinsing with ultra-pure water (UPW) for 10 min, immersing in diluted HF solution (1%) for 1 min, and rinsing again with UPW for 10 min. All of the chemicals used in this study were of reagent grade and used as received. Pt, Ir and Pd needles with a diameter of 200 μm were purchased from Nilaco Co. and used for making pores in the Si wafers. The ends of these metal needles were smoothed with emery paper and abrasives. In addition, tapered Ir needles, which were supplied by Tanaka Kikinzoku Co., were used as electrodes. The tapered length and base and tip diameters were 1 mm, 100 μm, and 50 μm, respectively.

The pore formation in Si wafers was performed with a standard electrochemical three-electrode system, the experimental setup of which is illustrated in Figure 1. The solution, in which Si wafers and electrodes were immersed, was 20 mol dm^{-3} HF. A Pt, Ir, or Pd fine needle was used as a working electrode and a Pt foil was used as a counter electrode. An Ag/AgCl electrode set in a plastic tube, which was filled with saturated KCl solution, was used as a reference electrode (hereafter referred to as Ag/AgCl). The needle electrode was fixed with a Teflon holder and brought into contact with a Si sample. The length of the needle electrode protruding from the holder was about 1.0 mm. The holder gave a loading of 65 g (for needles with a diameter of 200 μm) or 20 g (for the tapered Ir thin needles with a diameter of 50 μm at the tip) on the Si sample. The needle electrode was anodically polarized with an ALS 700C potentiostat. The electrochemical process was carried out in the dark at room temperature in the HF solution without stirring. Since HF is a very hazardous reagent, the processes were carried out in a fume hood equipped with a scrubber. After the electrochemical process, the Si sample was rinsed with UPW and dried in air. The morphologies of the pores generated in Si were observed with a Hitachi S-5000 scanning electron microscope (SEM). The depth profiles of the pores were analyzed with a KEYENCE VK-9700 laser scanning microscope.

3. RESULTS AND DISCUSSION

Pore Formation in Si Wafers Using a Pt Needle Electrode. Pores were formed in a Si wafer by applying constant anodic potentials to a Pt needle electrode with a diameter of 200 μm in 20 mol dm^{-3} HF solution. Figure 2 shows typical SEM images of p-type Si wafers with a resistivity of 12 Ω cm (p-Si-12) after processing at various potentials for 1 h. When the anodic potential

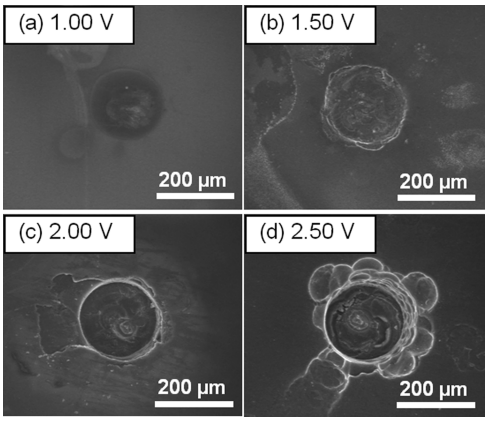

Figure 2. SEM images of pores formed in p-type Si wafers (12 Ω cm) by processing for 1 h in 20 mol dm^{-3} HF with a Pt needle electrode with a diameter of 200 μm at various potentials between 1.00 and 2.50 V vs. Ag/AgCl. The potentials are shown in the images. The depths of the pores are about (a) 2, (b) 20, (c) 110, and (d) 190 μm, which were determined with a laser scanning microscope.

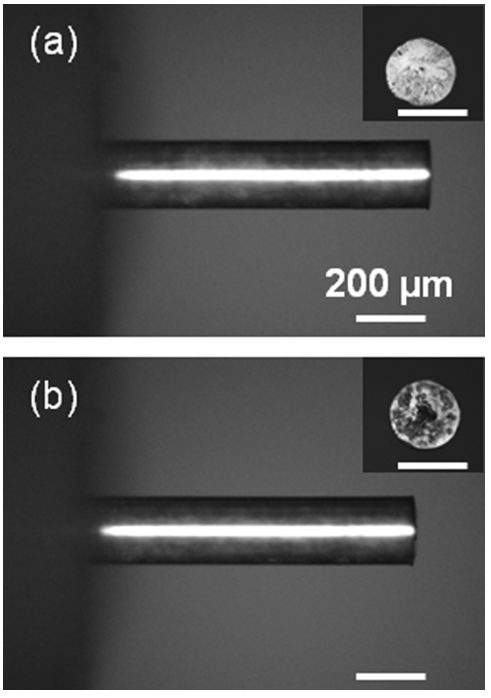

Figure 3. Images of a typical Pt electrode obtained through an optical microscope (a) before and (b) after making a pore in a p-type (12 Ω cm) Si wafer at 2.25 V vs. Ag/AgCl for 1 h. The insets show the surfaces of the tips. The scale bars represent a distance of 200 μm.

applied to the Pt needle electrode was 1.00 V vs. Ag/AgCl, very shallow dents were formed, as shown in Figure 2a. Appreciable pores as deep as 20 μm were formed when a potential of 1.50 V vs. Ag/AgCl was applied to the needle electrode, as shown in Figure 2b. This is consistent with the fact that electrochemical grooving of Si with Pt wire electrodes starts at around this potential.[21]

A deeper pore was formed by processing at a potential of 2.00 V vs. Ag/AgCl (Figure 2c). As shown in Figure 2d, a further increase in the applied potential up to 2.50 V vs. Ag/AgCl induced

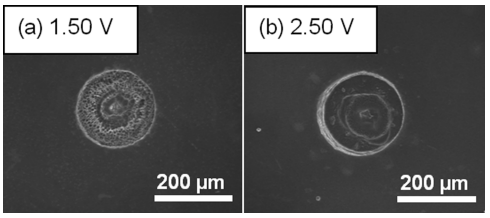

Figure 4. SEM images of pores formed in n-type Si wafers (11 Ω cm) by processing for 1 h in 20 mol dm^{-3} HF with a Pt electrode with a diameter of 200 μm at (a) 1.50 and (b) 2.50 V vs. Ag/AgCl. The depths of the pores are about (a) 40 and (b) 240 μm, which were determined with a laser scanning microscope.

intense corrosion of Si around the pore. In addition, the surface of the Si wafer became dark after the process at such a highly anodic potential. This color change is attributable to the formation of a PS layer on the surface, which is formed when positive holes (hereafter we call them holes) are supplied to the Si/HF solution interface at certain rates.[11] The corrosion of Si and the formation of a PS layer on p-type Si wafers therefore suggest that, at highly anodic potentials, holes are injected from the Pt needle electrode into the Si bulk, which then diffuse to the Si/HF solution interface.

No noticeable change is observed in the morphology of the Pt electrode used for making pores in Si at 2.25 V vs. Ag/AgCl, as shown in Figure 3, except for its end plane at which the Pt electrode was in contact with the Si sample. The end plane after the processing is roughened to some extent, as shown in the inset of Figure 3b. Such a morphological change of the plane was not observed when the same potential was applied to a Pt electrode without bringing it into contact with Si. These results suggest that some chemical interaction took place between Pt and Si during the electrochemical process. When anodic potential of 3.00 V vs. Ag/AgCl was applied to a Pt electrode in HF solution, the Pt electrodes became slightly thinner after processing for 1 h. This suggests that Pt dissolves gradually into HF solution at such a high anodic potential. Hence, in the following experiments, we did the experiments at potentials below 3.00 V vs. Ag/AgCl.

Formation of the pores in Si suggests that the electrochemical etching of Si selectively proceeds at the interface between the tip of the Pt electrode and the Si surface. The etching reaction of Si in HF solution is represented by

$$Si + 4h^+ + 6HF \rightarrow SiF_6^{2-} + 6H^+ \quad (1)$$

where h^+ stands for a hole supplied to Si. This reaction takes place when etching (or so-called electropolishing) of Si proceeds in HF solution.[24]

When an n-type Si wafer with a resistivity of 11 Ω cm (n-Si-11) was used instead of p-Si-12, the morphology of the pores was somewhat different from that of pores formed in p-type Si. The pore formed in n-Si-11 after processing for 1 h at an anodic potential of 1.50 V vs. Ag/AgCl was sharper and deeper (about 40 μm), as shown in Figure 4a, than the pore formed in p-Si-12 (about 20 μm) at the same potential (Figure 2b). When pores were formed by processing for 1 h at a potential of 2.50 V vs. Ag/AgCl, the depth of the pores reached about 240 μm for n-Si-11 and 190 μm for p-Si-12. It is notable that there is little corrosion around the pore formed in n-Si-11 (Figure 4b), in contrast to the case of p-Si-12 (Figure 2d). Furthermore, formation of a PS layer was suppressed on the surface of n-Si-11, as evidenced by very weak color change after the

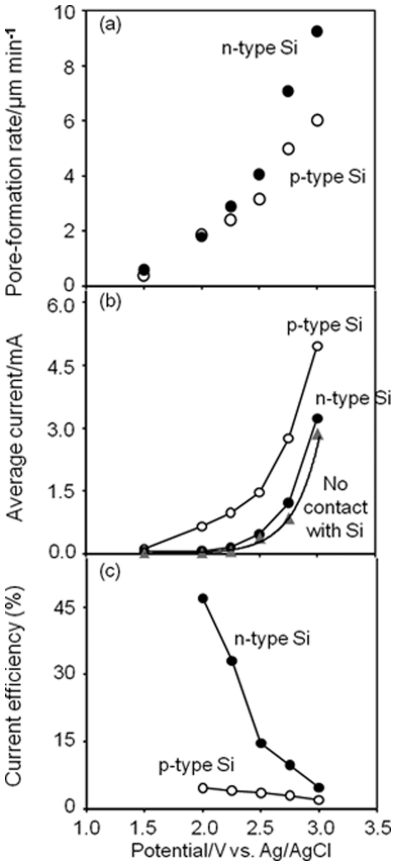

Figure 5. Formation of pores in p-type (12 Ω cm, open circles) and n-type (11 Ω cm, closed circles) Si wafers with a Pt electrode with a diameter of 200 μm as a function of anodic potentials applied to the Pt electrode in 20 mol dm^{-3} HF; (a) rates of pore formation, (b) average currents during the process and (c) current efficiencies for pore formation. At 1.50 V vs. Ag/AgCl, currents and volumes of the pores were too small to determine the current efficiency accurately. Triangles in (b) represent the currents observed at the Pt electrode that was not in contact with a Si wafer in the solution.

electrochemical process. The mechanistic difference in the pore formation in p-type and n-type wafers will be discussed later.

The effects of the anodic potential on pore formation rates and electric currents during the process were examined to elucidate the pore formation and corrosion in more detail. The pore formation rates for both p-Si-12 and n-Si-11 increased monotonously with increase in the applied potential (Figure 5a). The currents during the pore formation process also increased monotonously with increase in the applied potential, as shown in Figure 5b. Because the current fluctuated to some extent during the process, the average current (total charge/process time) is shown in this figure. Typical current profiles during the processing are shown in Supporting Information. The pore formation rates for p-Si-12 were lower than those for n-Si-11, although the currents were much larger for the former than for the latter, as shown in Figure 5b.

From the volumes of the pores formed in Si wafers and the currents, the current efficiencies for formation of the pores (η) are determined from the following equation,

$$\eta = 4 \times \text{volume of a pore} \times \text{density of Si atoms/number of electrons flowed} \quad (2)$$

in which corrosion around the pores is not included in the

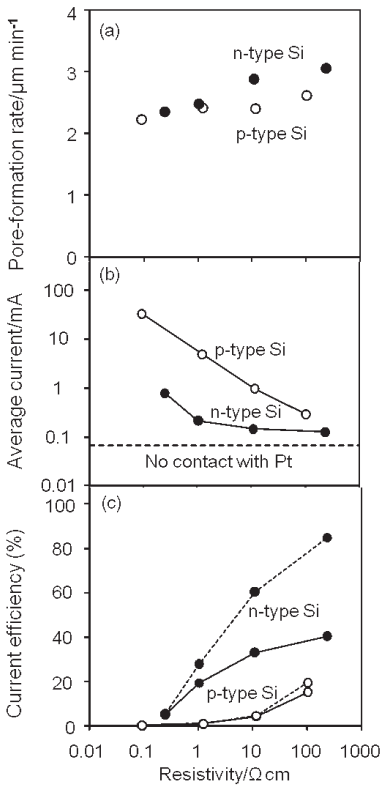

Figure 6. Formation of pores in p-type (open circles) and n-type (closed circles) Si wafers with a Pt electrode with a diameter of 200 μm as a function of resistivities of the wafers; (a) rates of pore formation, (b) average currents during the process, and (c) current efficiencies for pore formation. A potential of 2.25 V vs. Ag/AgCl was applied to the Pt electrode in 20 mol dm^{-3} HF. The dotted line in (b) represents the current observed at the Pt electrode that was not in contact with a Si wafer in the solution. The dotted lines in (c) represent the current efficiencies calculated after subtracting this blank current.

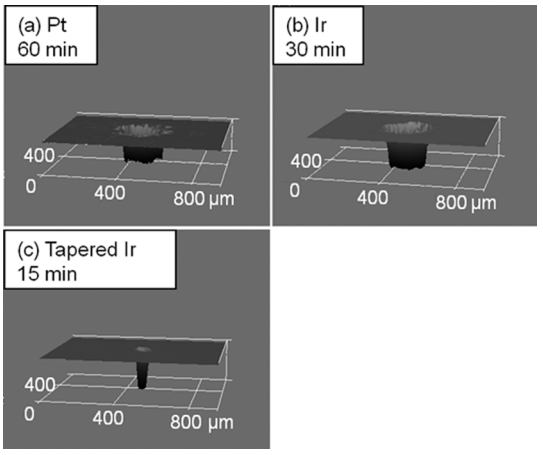

Figure 7. Three-dimensional images of pores formed in p-type Si wafers (12 Ω cm) using different needle electrodes; (a) a Pt electrode with a diameter of 200 μm, (b) an Ir electrode with a diameter of 200 μm, and (c) a tapered Ir electrode with a diameter of 50 μm at the tip. A potential of 2.25 V vs. Ag/AgCl was applied to the electrodes in 20 mol dm^{-3} HF. Process times are shown in the images.

volume of the pores because the volume of a pore is defined as the cross-sectional area of the electrode multiplied by the depth of the pore .

The calculated η for p-Si-12 and n-Si-11as a function of the electrode potential is shown in Figure 5c. For the n-Si-11 sample, the efficiency is about 50% at 2.00 V vs. Ag/AgCl and decreases as the potential increases from 2.00 to 3.00 V vs. Ag/AgCl. On the other hand, for the p-Si-12 sample, the efficiency is below 6% and decreases with increase in the potential. The currents not used for pore formation were used for corrosion of Si around the pores, formation of PS layers, and oxidation of water. Even when the Pt electrode was not brought into contact with Si, currents were observed over the potential region, as shown by triangles in Figure 5b. The currents are attributable to oxidation of water, which contribute to the decreased current efficiency for pore formation at high potentials. However, the low current efficiency of p-type Si wafers at potentials below 2.50 V vs. Ag/AgCl is mostly due to the corrosion of Si and the formation of PS layers.

The effects of resistivity of the Si wafers of both p-type and n-type on the pore formation rate and the current were also studied using Si samples with different resistivities. For the measurements, the potential applied to the Pt needle electrode was fixed at 2.25 V vs. Ag/AgCl. Figure 6a shows that the pore formation rates are not greatly affected by the resistivity or by the conductivity type. More precisely, the rate increases slightly with increase in resistivity, which is somewhat more evident for n-type Si wafers. On the other hand, the current flow during the electrochemical process decreases drastically with increase in resistivity, as shown in Figure 6b. These tendencies mean that the current efficiency for the formation of pores increases with increase in resistivity. In the case of n-type Si, more than 20% of current is used for the formation of pores if the resistivity is higher than about 1 Ω cm, and the efficiency further increases with increase in resistivity, as shown in Figure 6c. The current due to oxidation of water at the Pt needle electrode was 0.066 mA at this potential (2.25 V vs. Ag/AgCl). By subtracting this current, the current efficiency for the n-type samples with resistivities higher than 10 Ω cm is higher than 60%, as shown by a broken line in Figure 6c. This suggests that most of the holes are not injected into the bulk of these samples but are used for oxidation of Si atoms at the Pt/Si interface. On the other hand, in the case of p-type Si, the efficiency was very low unless the resistivity was higher than about 10 Ω cm. This suggests that holes diffuse easily into the bulk of p-type Si, which then causes corrosion of Si and formation of a PS layer at the Si/HF solution interface. The mechanism of pore formation will be discussed in more detail later.

Making Pores and through-Holes in Si Wafers Using Pt, Ir, or Pd Electrodes. Figure 7 shows three-dimensional images of pores obtained using Pt and Ir needles with a diameter of 200 μm and a tapered Ir needle with a diameter of 50 μm at its tip as electrodes. The wafers employed were p-Si-12 and the applied potential was fixed at 2.25 V vs. Ag/AgCl. The use of the Pt needle electrode enabled pore formation in this Si wafer at a rate of about 2.4 μm min^{-1} and a pore with a depth of about 140 μm was formed after processing for 1 h (Figure 7a). When an Ir needle electrode with a diameter of 200 μm was used, the pore formation rate was more than two-times faster; a pore with a depth of about 210 μm was formed after processing for 30 min (Figure 7b), and the pore formation rate was about 7.0 μm min^{-1}. The difference in the rates is attributed to the different catalytic activities of the metals for oxidizing Si at the Si/metal interface or injecting holes into the valence band. It is interesting to note that shallow dents were formed with a Pd needle electrode at a

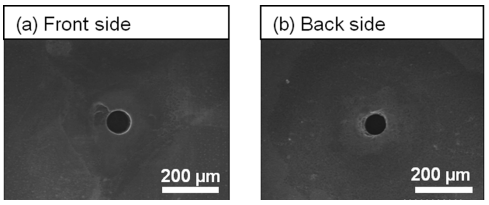

Figure 8. SEM images of a through-hole formed in a 250-μm-thick Si wafer (ca. 100 Ω cm) with a tapered Ir electrode with a diameter of 50 μm at the tip, to which 2.25 V vs. Ag/AgCl was applied for about 7.5 min in 20 mol dm^{-3} HF; (a) a front view and (b) a back view of the through-hole.

potential as low as 0.2 V vs. Ag/AgCl, which is above the top of the valence band of Si (about 0.5 V vs. Ag/AgCl). However, because Pd dissolved into HF solution gradually at higher potentials, we used Pt and Ir electrodes for making deep pores and through-holes in Si wafers.

The pore formation rate was enhanced when a tapered Ir needle with a diameter of 50 μm at the tip was used. The pore formed by using this electrode reached about 230 μm after a 15 min electrochemical process at 2.25 V vs. Ag/AgCl, as shown in Figure 7c; the boring rate was about 15 μm min^{-1}. In addition, using the 50 μm tipped Ir needle, through-holes were formed in a 250 μm-thick p-type Si (100 Ω cm) wafer in about 7.5 min at the applied potential of 2.25 V vs. Ag/AgCl: the average boring rate was 33 μm min^{-1}. Figure 8 shows typical SEM images of the pores observed at the front and back sides of the wafer. The diameters of the through-holes were about 80 and 70 μm at the front and back sides, respectively. The difference in the diameters reflects the tapering of the Ir electrode. The Si sample was hardly corroded near the through-hole. When we processed a 625 μm-thick n-type Si wafer (11 Ω cm) with the tapered Ir electrode, a through-hole was formed in about 14 min: the average boring rate reached 46 μm min^{-1}. We expect that the rate of pore formation can be further increased and the diameter of through-holes can be decreased by using an Ir needle with a sharper tip. The time needed for making the through-holes can be shortened by increasing the anodic potential.

The significant improvement in the pore formation rate using the tapered Ir needle with a 50 μm tip is partly due to high pressure applied to the Ir/Si interface due to the small contact area. Such an effect by increased pressure was also observed in grooving Si ingots.[23] Presumably, the high pressure is useful to crush the PS layer formed at the electrode/Si interface because the PS layer impedes the reaction at the interface. The small contact area at the tip of the fine electrode may also be useful to exchange solution at the electrode/Si interface, which is necessary for dissolution of Si.

Mechanism of Pore Formation in Si. Silicon dissolves oxidatively into HF solution by the reaction represented by eq 1. The standard electrode potential of the reaction (E^0) is −1.24 V vs. SHE[25] or −1.44 V vs. Ag/AgCl. This means that thermodynamically Si can dissolve into HF solution as hydrogen evolves from the solution. By careful analysis, it is possible to detect hydrogen evolution as Si dissolves into HF solution or pure water.[26] However, this reaction is usually negligibly slow. Under anodic bias, p-type Si in HF solution is oxidized by holes existing in the valence band. This leads to dissolution (or electropolishing) of Si into HF solution or formation of a PS layer on the surface, which depends on the electrode potential and the concentration of HF.[24,27] The dissolution and PS layer formation also occur on the surface of n-type Si under photoirradiation, which is necessary for supplying holes to the surface. The dissolution and PS layer formation may be intermediated by SiO_2, as is often discussed in the mechanism of metal-assisted etching.[11]

In the present system, Si is not connected to an external circuit through an Ohmic contact, which is normally formed at the backside of a wafer, but brought into contact with the needle electrode. Hence, the Si/metal contact plays an important role in the pore formation mechanism. We can think of two simplified models for the Si/metal contact, which need modification as discussed later. One is a direct contact between Si and the metal (or a Schottky junction). In the other model, the metal and Si are separated by a very thin layer of HF solution. In the former model, the relative energy levels of Si and the metal are not affected by the potential of the electrode, whereas they are in the latter model. The fact that the pore formation rate is affected by the potential of the electrode seems to be favorable to the second model. However, by the second model, it is difficult to explain the result that the pore formation rate is affected by the kinds of metals.

It is reasonable to consider that the etching reaction (or pore formation) does not proceed at the Si/solution or Si/metal interface, but it proceeds at the circumferences of the contact areas, as schematically shown in Figure 9. Hence, the relative energy levels of the electrode and Si at the circumference of the contact area are critical in discussing the etching mechanism. To deepen the understanding of the energy structure in this region, it is meaningful to begin the discussion with the energy diagrams of the Si/HF solution and Si/metal junctions because they affect the energy structure in the circumference region. The energy diagrams of p-type Si/solution and n-type Si/solution junctions are schematically shown in panels a and d in Figure 10, in which the E^0 level of eq 1 is also shown. The energy diagrams of p-type Si/metal and n-type Si/metal junctions, where no voltage is externally applied to the metal, are shown in panels b and e in Figure 10. The dotted lines in the figures represent the diagrams for the contact with a small-work-function metal.

When an anodic potential is applied to the metal, the energy levels of Si near the Si/metal junction shift downward, as shown in panels c and f in Figure 10. We supposed that the Fermi level of Si is determined by the properties of the Si/HF solution interface because the Si/metal contact area is much smaller than that of the Si/solution interface. In real systems, the Fermi level should be perturbed by a small change in the environment because it is not controlled externally. However, if holes are injected from the metal into the bulk of Si under application of highly anodic potential to the metal, the Fermi level of whole Si shifts downward.

An important point in the present process is that a three-phase (Si/metal/solution) boundary is formed on the Si surface, when a needle electrode is brought into contact with Si. At the metal/solution interface, a strong electric field is formed in solution near the metal to which an electric potential is applied because of the formation of an electric double layer. The electric field develops to a depth of about 0.5 nm from the metal surface;[28] the distance depends on the ionic strength of the solution. On the other hand, the space charge layer in Si develops to a depth of some hundreds nm. Figure 11a shows the energy diagram represented by contour line near the 3-phase boundary, in which an anodic potential is applied to the metal. Because of the strong electric field formed in solution near the metal, a strong electric field is also formed in Si near the 3-phase boundary along the Si/solution interface to a distance of about 0.5 nm, as shown by solid contour lines in Figure 11a. The energy diagrams along Line A

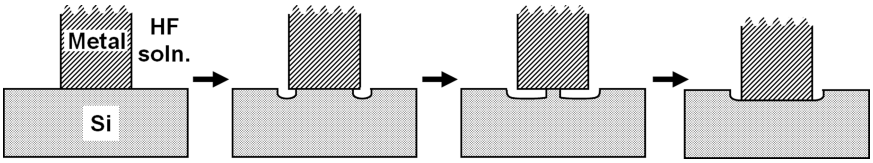

Figure 9. Schematic cross-sectional images of Si/metal interface, which represent sequential steps of pore formation in Si by a metal electrode to which an anodic potential is applied in HF solution.

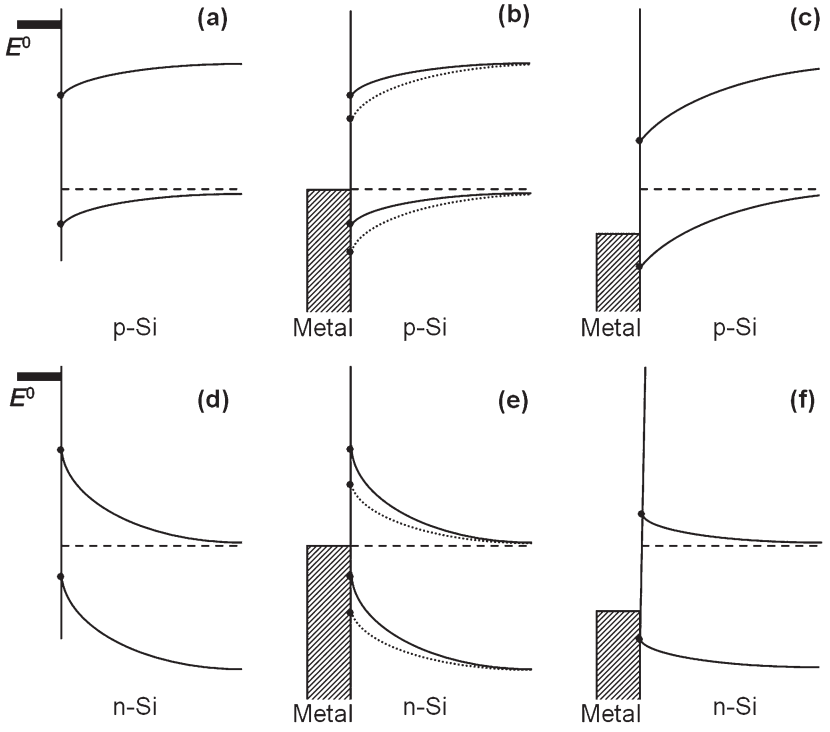

Figure 10. Schematic energy diagrams for (a) p-type Si/solution, (b, c) p-type Si/metal, (d) n-type Si/solution, and (e, f) n-type Si/metal interfaces. In the diagrams c and f, an anodic potential is applied to the metal against a counter electrode (not shown). Dotted lines in b and e represent the energy profiles for the junctions with a low-work-function metal. E^0 stands for the thermodynamical potential for dissolution of Si.

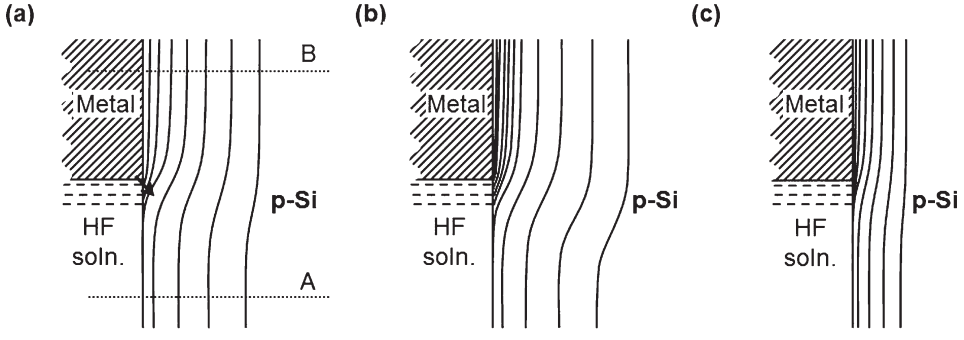

Figure 11. Schematic energy diagrams represented by contour lines for the area near the p-type Si/metal/solution boundary; (a, b) high-resistivity p-type Si and (c) low-resistivity p-type Si. A large Schottky barrier height (or a low work function of the contacting metal) is assumed for (b). The arrow in (a) indicates hole injection into the valence band of Si. The magnification of the *y* axis is much larger than that of the *x* axis. The potential profiles along Line A and Line B in a correspond to the energy diagrams shown in panels a and c in Figure 10, respectively.

and Line B in Figure 11a correspond to those shown in panels a and c in Figures 10, respectively. The high density of contour lines in Si near the three-phase boundary means that strong electric field is developed there. Similar energy diagrams for semiconductors, on which metal particles are loaded, in electrolyte solution have been proposed by Nosaka et al.[29] and Nakato et al.[30] Because of the strong electric field produced near the three-phase boundary by the electric double layer formed in solution, the energy levels of Si are lowered near the anodically biased metal. Hence, when a potential more anodic than a certain

level is applied to the needle electrode, the Fermi level of the metal can be more positive than the top of the valence band of Si at places within a distance of electron tunneling (about 1 nm). This leads to hole injection from the metal to p-type Si, as shown by an arrow in Figure 11a. When a metal with a smaller work function is brought into contact with Si, the energy levels of p-type Si near the metal become lower, as discussed above. This in turn lowers the energy levels of Si near the 3-phase boundary and makes it more difficult to inject holes into the valence band, as shown in Figure 11b. Contrarily, it becomes easy to inject holes into the valence band using metals with large work functions. Therefore, the different pore formation properties of different metal electrodes should be related to the difference in their work functions. However, it must be noted that formation of silicides or alloys at the interface strongly affects the Schottky barriers.[31] This obscures the correlation between the work functions of metals and the pore-formation properties.

Figure 9 illustrates the consecutive steps of pore formation in Si with a needle electrode. First, holes are injected from the needle electrode into the valence band of Si near the 3-phase boundary by the above-mentioned mechanism. Second, the holes oxidize Si near the boundary area and the Si dissolve into HF solution. Third, as a result, the 3-phase boundary moves back. Finally, when all the Si atoms at the original interface are dissolved, the needle electrode moves downward. The pores are formed in Si by repeating the steps. In a real process, we consider that there are many tiny contact areas at a Si/electrode interface and the dissolution occurs from their circumferences.

Here, we consider the current efficiency for pore formation (η), which was defined by eq 2. The efficiency is below 1 because part of current is not used for making pores in Si. Considering possible competitive processes, η is expressed by

$$\eta = Q_p/Q_T = 1 - (Q_c + Q_{PS} + Q_w)/Q_T \qquad (3)$$

where Q_T is the total charge flown at the needle electrode and Q_p, Q_c, Q_{PS}, and Q_w are the charges used for pore formation, corrosion of Si surface over the region wider than the cross section of the needle electrode, formation of the PS layer, and oxidation of water, respectively.

Holes injected into n-type Si are more likely to stay near the 3-phase boundary than those injected into p-type Si because of the upward band bending in n-type Si, as shown in Figure 10d–f. This will lead to high η for n-type Si, which is consistent with the results shown in Figures 5c and 6c. However, with an increase in the anodic potential, holes are injected at a rate higher than the rate of their consumption near the three-phase boundary. The excessive holes move along the n-type Si/solution interface due to the potential profile at the interface, as shown in Figure 10d. This results in the formation of the PS layer and corrosion of Si beyond the Si/electrode contact area. At potentials higher than 2.50 V vs. Ag/AgCl, a considerable part of current is also used for oxidation of water, as shown in Figure 5b. This leads to further decrease in η.

In the case of p-type Si, some holes injected into Si are captured by Si atoms at the Si/solution interface and are used for dissolution of Si atoms. However, some holes migrate into the bulk of Si because of the electric field developed near the Si surface, as shown in Figure 10c. This leads to lowering of the Fermi level of the whole Si sample. If the flux of injected holes is large, the Fermi level shifts to such a low level as to allow oxidation of Si over the whole sample surface. This is consistent with the result that a PS layer is likely to be formed on p-type Si when an anodically polarized needle electrode is brought into contact with Si in HF solution.

The η value was also dependent on the resistivity p-type and n-type Si samples, as shown in Figure 6c. With decrease in the resistivity (or increase in the acceptor density) of p-type Si samples, the current during the pore formation process increased drastically, as shown in Figure 6b. This is attributable to formation of stronger electric field near the 3-phase boundary in low-resistivity Si (Figure 11c), which enhances hole injection into the bulk of Si. For the same reason, hole injection into the valence band of n-type Si is enhanced with decrease in the resistivity (or increase in the donor density). If holes are excessively injected into n-type Si, the holes migrate along the Si surface, resulting in the formation of a PS layer and corrosion of Si around the pore, although it is limited compared with the case of p-type Si. This is responsible for the lowered η for low-resistivity n-type Si, as shown in Figure 6c.

The mechanism of the electrochemical pore formation in S must be closely related to the mechanism of metal-assisted etching of Si.[11] In the metal-assisted etching, oxidants such as hydrogen peroxide are added to HF solution. The oxidants accept electrons from the metal particles and give anodic potentials to them, leading to formation of pores by the electrochemical process at places where the metal particles are loaded.[11] Hence, we consider that the model shown above is closely related to the metal-assisted etching of Si.

Although further study is necessary, we consider that a mechanism different from the above-mentioned mechanism may also contribute to the pore formation in Si and metal-assisted etching when Pd is used as the electrode or catalyst. With a Pd needle electrode, a shallow dint was formed even at a potential more negative than the top of the valence band, as mentioned above. This result cannot be explained by the mechanism discussed above. In metal-assisted etching of Si, Yae et al.[32] reported unique property of Pd particles, with which they observed pore formation in Si in solution that did not contain any strong oxidants. These results obtained with a Pd electrode and Pd particles must be closely related. The mechanisms of these phenomena are under investigation in our group.

4. CONCLUSION

In the present study, we have reported pore formation in Si wafers using anodically polarized metal needle electrodes in HF solution. The pore formation rate and the morphology of the pores are significantly influenced by applied potentials, conductivity types and resistivity of Si wafers, and metals used as the electrodes. It is easier to make sharp pores in n-type Si wafers at high current efficiency than in p-type Si wafers. The experimental results are explained by the model in which the 3-phase (Si/metal/solution) boundary plays an important role. On the basis of the collected parameters for the pore formation in Si, we succeeded in making a through-hole with a diameter of about 80 μm in Si wafers using a tapered Ir electrode with a tip diameter of 50 μm. Because the present method does not generate debris or cause thermal damage, it may be applicable not only to making through-holes but also to advanced micromachining of Si wafers. We consider that the model is useful for understanding the metal-assisted etching of Si, which is being studied by many research groups.

■ ASSOCIATED CONTENT

Supporting Information. Typical current patterns observed during the electrochemical process (Figure S1).

This material is available free of charge via the Internet at http://pubs.acs.org.

AUTHOR INFORMATION

Corresponding Author
*E-mail: matsu@chem-es.osaka-u.ac.jp. Fax: +81-6-6850-6699. Tel: +81-6-6850-6698.

ACKNOWLEDGMENT

This work was supported by a Grant-in-Aid for Scientific Research on Fundamental Research and by a Grant-in-Aid for Scientific Research on Priority Areas (no. 458) each from the Ministry of Education, Culture, Sports, Science and Technology, Japan. T.S. expresses his thanks to the Global COE (center of excellence) Program "Global Education and Research Center for Bio-Environmental Chemistry" of Osaka University for financial support.

REFERENCES

(1) Koyanagi, M.; Nakamura, T.; Yamada, Y.; Kikuchi, H.; Fukushima, T.; Tanaka, T.; Kurino, H. *IEEE Trans. Electron Devices* **2006**, *53*, 2799.
(2) Burns, J.A.; Aull, B.; Chen, C.; Keast, C.; Knecht, J.; Suntharalingam, V.; Warner, K.; Wyatt, P.; Yost, D. *IEEE Trans. Electron Devices* **2006**, *53*, 2507.
(3) Lang, W. *Mater. Sci. Eng.* **1996**, *R17*, 1.
(4) Coburn, J.W.; Winters, H.F. *J. Vac. Sci. Techn.* **1979**, *16*, 391.
(5) Rangelow, I.W. *Surf. Coat. Technol.* **1997**, *97*, 140.
(6) Ranganathan, N.; Lee, D.Y.; Ebin, L.; Balasubramanian, N.; Prasad, K.; Pey, K. L. *J. Micromech. Microeng.* **2008**, *18*, 115028.
(7) Müllenborn, M.; Dirac, H.; Petersen, J.W. *Appl. Surf. Sci.* **1995**, *86*, 568.
(8) Yuan, W.; Ma, B. *J. Mater. Process. Technol.* **2008**, *200*, 390.
(9) Allongue, P.; Jiang, P.; Kirchner, V.; Trimmer, A.L.; Schuster, R. *J. Phys. Chem. B* **2004**, *108*, 14434.
(10) Schuster, R.; Kirchner, V.; Allongue, P.; Ertl, G. *Science* **2000**, *289*, 98.
(11) Huang, Z.; Geyer, N.; Werner, P.; de Boor, J.; Gösele, U. *Adv. Mater.* **2011**, *23*, 285.
(12) Tsujino, K.; Matsumura, M. *Electrochem. Solid-State Lett.* **2005**, *8*, C193.
(13) Lee, C.-L.; Tsujino, K.; Kanda, Y.; Ikeda, S.; Matsumura, M. *J. Mater. Chem.* **2008**, *18*, 1015.
(14) Tsujino, K.; Matsumura, M. *Electrochim. Acta.* **2007**, *53*, 28.
(15) Tsujino, K.; Matsumura, M. *Adv. Mater.* **2005**, *17*, 1045.
(16) Peng, K.Q.; Yan, Y.J.; Gao, S.P.; Zhu, J. *Adv. Mater.* **2002**, *14*, 1164.
(17) Peng, K.; Wu, Y.; Fan, H.; Zhong, X.; Xu, Y.; Zhu, J. *Angew. Chem. Int. Ed.*. **2005**, *44*, 2733.
(18) Huang, Z.; Zhang, X.; Reiche, M.; Liu, L.; Lee, W.; Shimizu, T.; Senz, S.; Gösele, U. *Nano Lett.* **2008**, *8*, 3046.
(19) Fan, H.; Li, X.; Song, S.; Xu, Y.; Zhu, J. *Nanotechnology* **2008**, *19*, 255703.
(20) Peng, K.; Jie, J.; Zhang, W.; Lee, S.T. *Appl. Phys. Lett.* **2008**, *93*, 033105.
(21) Lee, C.-L.; Tsujino, K.; Kanda, Y.; Hirai, T.; Ikeda, S.; Matsumura, M. *J. Electrochem. Soc.* **2009**, *156*, H134.
(22) Salem, M.S.; Lee, C.-L.; Tsujino, K.; Ikeda, S.; Matsumura, M. *J. Mater. Process. Technol.* **2010**, *210*, 330.
(23) Lee, C.-L.; Kanda, Y.; Ikeda, S.; Matsumura, M. *Sol. Energy Mat. Sol. Cells* **2011**, *95*, 716.
(24) Turner, D.R. *J. Electrochem. Soc.* **1958**, *105*, 404.
(25) *CRC Handbook of Chemistry and Physics*, 81st ed.; Lide, D.R., Ed.; CRC Press: Boca Raton, FL, 2000.
(26) Sawada, Y.; Tsujino, K.; Matsumura, M. *J. Electrochem. Soc.* **2006**, *153*, C854.
(27) Lehmann, V. *Electrochemistry of Silicon*: Wiley-VCH: Weinheim, Germany, 2002.
(28) Morrison, S.R. *Electrochemistry at Semiconductor and Oxidized Metal Electrode*; Plenum Press: New York, 1980; Chapter 2.
(29) Nosaka, Y.; Ishizuka, Y.; Miyama, H. *Ber. Bunsen Ges. Phys. Chem.* **1986**, *90*, 1199.
(30) Nakato, Y.; Ueda, K.; Yano, H.; Tsubomura, H. *J. Phys. Chem.* **1988**, *92*, 2316.
(31) *Metal-Semiconductor Schottky Barrier Junctions and Their Applications*; Sharma, B.L., Ed.; Plenum Press: New York, 1984.
(32) Yae, S.; Tashiro, M.; Abe, M; Fukumuro, N.; Matsuda, H. *J. Electrochem. Soc.* **2010**, *157*, D90.